CRACK GROWTH MONITORING AND FATIGUE ANALYSIS FOR CARBON-FIBER REINFORCED POLYMERS USING ULTRASONIC INSPECTION AND COHESIVE ZONE MODELING

Khaled Matalgah, Yuqing Zhao, Douglas E. Smith, Trevor J. Fleck
Department of Mechanical Engineering, Baylor University, One Bear Place, #97356, Waco, TX, 76798-7356, USA
Keywords: CFRP; Delamination; Mode-II; Fatigue; Ultrasonic Testing; Prediction Modelling

Abstract

Carbon Fiber-Reinforced Polymers (CFRPs) are extensively used in various applications which include the aerospace, automotive, and civil engineering industries, among others. Fatigue crack growth is one of the main causes of premature failure in aircraft structural components. Therefore, predicting fatigue life is essential to avoid catastrophic failure. The detection of any subsurface flaws that arise either during manufacturing or service use are critical to avoid component failures. Non-destructive testing (NDT) is commonly used to evaluate CFRP components without causing damage providing insights into the structural integrity of these components. In this paper, CFRP end-notched flexure (ENF) samples were tested via the 4-point bend test setup, to observe and predict stable crack propagation. The extent of crack propagation was monitored via ultrasonic inspection at various stages of the fatigue testing process. Various stages of delamination damage measured via ultrasound served as into our ENF ABAQUS Finite Element Analysis model, which was subsequently used to simulate future crack growth under fatigue loading. Simulation results of fatigue crack growth compared well with experimentally measured fatigue damage.

Introduction

Carbon-Fiber Reinforced Polymers (CFRPs) have emerged as a versatile and high-performance material in various industries such as automotive and aerospace [1]. This increased usage of CFRPs is due to their advantageous properties such as, high strength-to-weight ratio, excellent stiffness and rigidity, and design flexibility [1], [2]. Despite their beneficial properties, fatigue damage can accelerate quickly posing a significant challenge in high stress cyclically loaded designs. Fatigue damage in automotive applications caused by the dynamic and cyclic loading conditions experienced by vehicle components can lead to potential catastrophic failure [3]. A variety of vehicle components are manufactured by CFRP. This includes chassis and suspension components. Cyclic loading experienced by road vibrations can lead to the initiation and propagation of fatigue cracks in those said components, leading to progressive damage which could eventually lead to failure of these components [4]. It is, therefore, critical to accurately identify crack formation and growth, as well as predict the subsequent fatigue life of damaged CFRP components.

Detecting and evaluating delaminations in CFRP components poses a significant challenge due to their sub-surface nature. Accurate measurement and prediction of the subsurface damage is crucial for ensuring the safe utilization of CFRP components and predicting their future in-service performance. The non-homogenous and anisotropic nature of CFRPs further complicates the detection and assessment process, necessitating the need for high-fidelity Nondestructive Testing (NDT) methods that can provide information about the extent and characteristics of delmainations [5].

Nondestructive testing has become a prevalent approach for evaluating the extent of delamination within CFRP components. These non-invasive methods are widely employed due to their ability to assess the structural integrity of CFRP components without causing further damage. NDT techniques offer valuable insights into the extent of delamination, helping in the determination of component health and potential failure risks [6]. Some NDT methodologies include eddy current testing (ECT), X-ray computed tomography (CT), infrared thermography (IR), and ultrasonic testing (UT). X-Ray CT is considered to be the most accurate, as it employs high-resolution imaging techniques to visualize internal structures with exceptional detail [7]. However, CT is expensive with limited accessibility, has size and portability restrictions, and is limited in terms of deployment in the field [8]. Ultrasonic testing (UT) is often favored over CT in specific applications due to its accessibility, portability, real-time inspection capabilities, cost-effectiveness, and surface accessibility. Also, UT remains capable of providing high-resolution imaging and accurately detecting small defects by utilizing high-frequency sound waves [9]. This high-fidelity data, with accurate quantification of the sub-surface crack in three spatial dimensions, is critical for subsequent predictive analytics in finite element analysis (FEA). In UT, a transducer emits high-frequency sound waves into the material in question via the pulse-echo scheme. In this approach, defects such as cracks within the material causes sound waves to scatter or reflect which are then detected by the same transducer. Sound intensity data is then used to analyze, identify, and characterize the presence of interlaminar cracks [10].

In addition to non-destructive testing (NDT), predictive modeling techniques have become invaluable and helpful tools for understanding and predicting fatigue growth in CFRP components under fatigue loading [11]. In this paper, ABAQUS is the software employed to evaluate advanced finite element analysis (FEA) models which have been developed to simulate the behavior of CFRP structures subjected to cyclic loading conditions. Paris law-based criteria and the cohesive zone method (CZM) finite element modeling techniques are widely used for modeling the fatigue crack propagation of composite materials that have a local crack where stress concentration exist [12]–[17]. Bak, B. L. V., et al. [18] provide a review of these methods which exposes the difficulties of applying these methods including the precise extraction of energy release rate of crack tip and the evaluation of the fatigue fracture process zone ahead of crack tip. Among these methods, the crack-tip-tracking advancement method [19] proposed by the researchers from Bristol University assumes that fatigue damage evolution is confined within the most opened crack tip element. In this way, one could dismiss the requirement of a fatigue fracture process zone length which is hard to be quantified from experimental testing. In this approach, the historical integrated energy release rate of the crack tip element is considered as the overall crack tip energy release rate.

This paper focuses on the monitoring (via UT) and prediction (via FEA) of fatigue crack growth for CFRP components. All samples were mechanically tested in fatigue via the 4-point bend fixture to induce stable delamination growth. Initial damage was induced via fatigue testing of the CFRP components. Ultrasonic testing was then performed to measure the crack front to obtain accurate data which subsequently served as input into our ABAQUS FEA fatigue crack growth simulation models. This damage was then considered as the starting point for predicting fatigue crack growth, which was simulated for additional 5,000 and 10,000 cycles. To validate the simulation results, experimental testing was conducted by subjecting the CFRP component to the same number of cycles via a 4-pt bend cyclic loading. UT was then performed after each test was completed to measure the crack front. Finally, both sets of results were compared and verified.

Materials and Methods

Specimen Fabrication

In this study, CFRP laminates were fabricated using unidirectional prepreg (Carbon Fiber +

250F Resin System) manufactured via a hot press (Carver, 3893L4PLI006), under the manufacturer's recommended temperature cycle and at a constant pressure of 40 psi, comprised entirely of 30 [0°] laminas. During manufacturing, a polytetrafluoroethylene (PTFE) film (McMaster-Carr, SF103V0002) of 50 µm thickness was inserted in the midplane of the laminate. The laminate was then cut via a tile saw, followed by grinding to smooth out the edges, into coupons of 180 x 25 mm, as shown in Figure 1, to follow the ASTM standard D7905 [20]. For both static and fatigue tests, mode-II fracture is the fracture mode in question. Mode-II is characterized by shear displacements occurring parallel to the crack plane, which leads to more complex crack propagation behavior when compared to mode-I fracture.

Mechanical Fatigue Test

Prior to the mechanical fatigue tests, three quasistatic tests of the particular sample geometry were conducted to determine the critical displacement (h_{max}) via a quasi- 4-pt bend test setup, as shown in Figure 1. The quasistatic tests were conducted using a universal test machine (Test Resources SM-1000-294) with a loading capacity of 4.4 kN. The test machine was operated in a displacement control mode with a constant displacement rate of 1 mm/min. The critical displacement from quasistatic testing, or the maximum displacement prior to unstable crack growth, was used in in subsequent fatigue tests, which were operated at to 50% of the critical displacement, resulting in a maximum deflection of 1.8mm. The samples were then mechanically fatigued to induce various amounts of initial damage, the geometry of which was accurately quantified in shape and dimension, which was used to define the initial crack location in the ABAQUS fatigue model. This initial damaged state was considered as the initial condition in the model and will be references as N = 0 cycles in this document. Fatigue tests were conducted using a universal testing machine (Test Resources, F2500-B), with Table 1 summarizing the pertinent testing parameter. All samples were tested to 5,000 cycles followed by another 5,000 cycles for a total of 10,000 cycles.

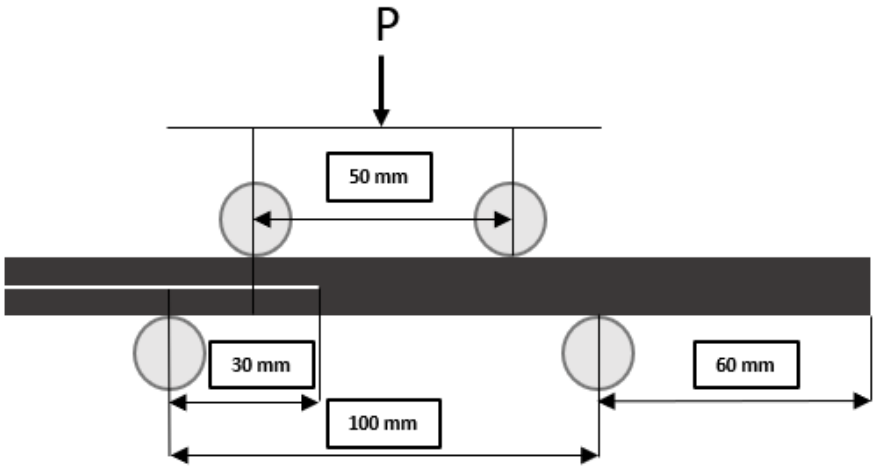

Figure 1. 4-pt Fatigue ENF Test Configuration.

Table 1. Mechanical Fatigue Testing Parameters

Sample	Frequency	Maximum Displacement	Minimum Displacement	Stress Ratio (min/max displacement)
F2	3 Hz	1.8 mm	0.18 mm	0.1
F4	3 Hz	1.8 mm	0.54 mm	0.3
F5	3 Hz	1.8 mm	0.9 mm	0.5

Ultrasonic Scanning Set Up

Ultrasonic C-scans were performed after initial damage, as well as after each subsequent set of fatigue tests, to monitor, measure, and analyze changes in the crack front within the test component. The UT scans were conducted using a custom pulse echo C-scan immersion system appearing in **Error! Reference source not found.**. A 10 MHz, 38.1 mm (1.5") nominal focal length, spherically focused transducer (A311S-SU-F1.5N-PTF, Olympus) was used. The transducer was focused at 50% depth into the sample since this was the anticipated depth of the delamination. During each scan, the transducer followed a raster pattern, as depicted in Figure 2(b), with 0.2 mm raster resolution in both the x_1 and x_2 directions, where x_1 aligning along the length of the sample and x_2 aligning transversely to x_1, as shown in Figure 2(a). After each UT scan was completed, a custom MATLAB script is was employed to analyze the UT data for automatic location and calculation of the crack front.

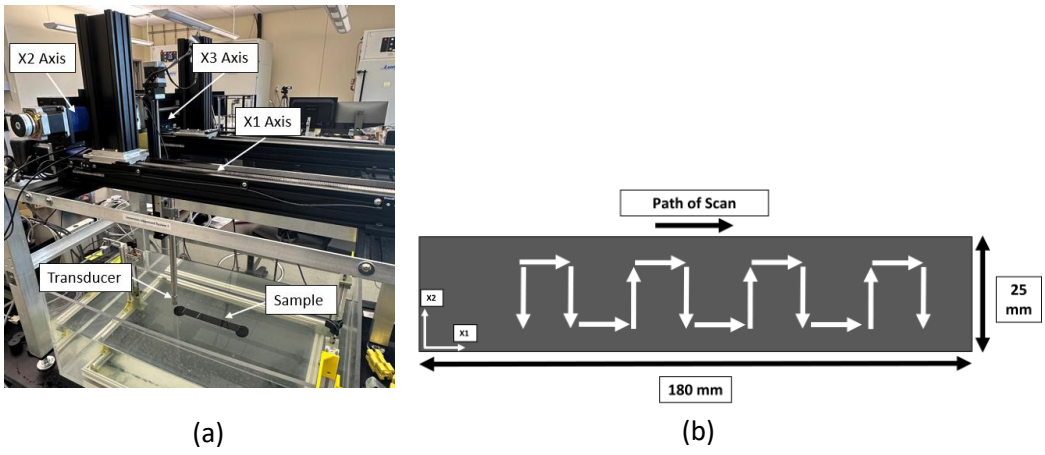

Figure 2. Ultrasonic Testing Set Up with (a) Custom UT Immersion System and (b) Representative Rastering Pattern (0.2 mm spacing used in all studies.

ABAQUS Modelling

The Mode II fatigue crack propagation in this paper is simulated by means of crack tip tracking method (CTTM) [19] and envelope loading method [21] in ABAQUS/Explicit. The geometry of the simulated 4-point bending $[0]_{30}$ laminates is identical to the experimental setup as shown in Figure 3. The cohesive interface shown in Figure 4 is comprised of cohesive elements inserted at the midplane of the $[0]_{30}$ laminates with an initial crack front determined from UT scan results as described above. The cohesive interface has a thickness of 1/10 of the unidirection composite

lamina layer. A bias mesh is applied to the upper and lower 0-degree plates with a total number

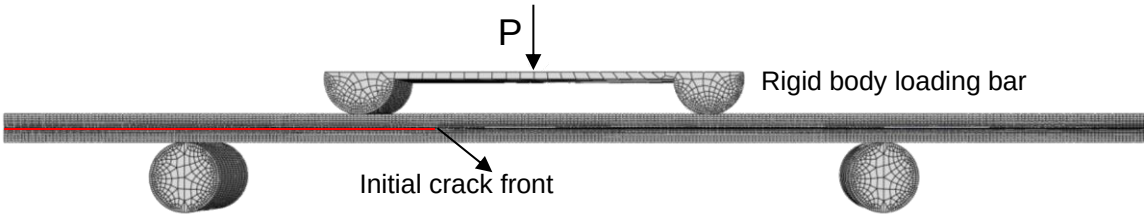

Figure 3. Finite element model in Abaqus.

Figure 4. Initial crack front determined from UT scan results.

of elements through the thickness direction of 10. The element size along the length direction for both 0-degree layers and cohesive layers is approximately 0.5 mm, while the width direction consists of 17 elements. It is assumed that the 0-degree layers are linear elastic during loading, while the cohesive interface follow bi-linear traction separation law. The properties used in the simulation appear in Table 2 and Table 3 [21].

Table 2. Elastic properties of orthotropic unidirectional composite.

E_{11} (GPa)	E_{22} (GPa)	E_{33} (GPa)	ν_{12}	ν_{13}	ν_{23}	G_{12} (GPa)	G_{13} (GPa)	G_{23} (GPa)
120	10.5	10.5	0.3	0.3	0.51	5.25	5.25	3.48

Table 3. Properties for cohesive element.

K_I (N/mm^3)	K_{II} (N/mm^3)	K_{III} (N/mm^3)	X_I (MPa)	X_{II} (MPa)	X_{III} (MPa)	G_{Ic} (N/mm)	G_{IIc} (N/mm)	G_{IIIc} (N/mm)
100000	100000	10000	30	60	60	0.2	1.002	1.002

In Table 3, K, X and G_c denote the initial stiffness, ultimate strength, and critical energy release rate of the cohesive interface respectively, and subscripts I, II and III indicate the failure mode of cohesive element.

Analysis

MATLAB Analysis

An in-house MATLAB script was developed to automatically measure and locate the spatial location of the crack front post UT scanning. This was done by analyzing the full waveform of locally averaged A-scans and looking at the abnormalities in the attenuation of the wave to find the depth. The A-scans are first smoothed and filtered using Gaussian smoothing functions. To ensure consistent reference points, the signals from each A-scan are shifted relative to the front wall, aligning them in time in order to prevent any image distortion arising during the component

testing. To focus on the specific depth of interest, in this case at the midplane, a gated C-scan is generated by creating a time window centered around the desired depth, the gate width is also changed to fit the material of interest. Within the time gate surrounding the midplane, the energy of the signal at each x_1, x_2 location was calculated resulting in the surface plot shown in Figure

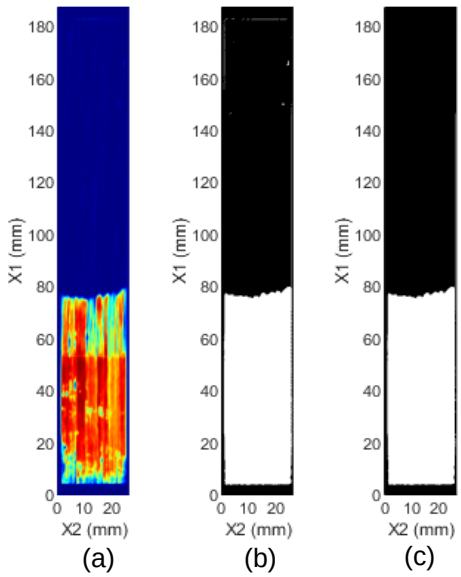

Figure 5. Images demonstrating the process steps of the 3-dimensional UT C-scan data, including (a) the original gated C-scan based on the energy of the signal in the gate, (b) the binarized C-scan, and (c) the final, filtered C-scan.

5(a). This image was then binarized based on a threshold determined by the average response of an undamaged region of the component, resulting in the image shown in Figure 5(b). This image was then filtered to remove any features below the delamination size of interest as shown in Figure 5(c).

Cohesive Zone Modeling

The cohesive traction separation law (TSL) is implemented into VUMAT user subroutine as the constitutive relation for the 4 integration point cohesive element COH3D8 to simulate the traction and separation between upper and lower surfaces of the cohesive interface. As denoted in CTTM, the most opened element which is typically the first element from the physical crack front along the crack propagation direction is tracked as the crack tip element. In the VUMAT, the

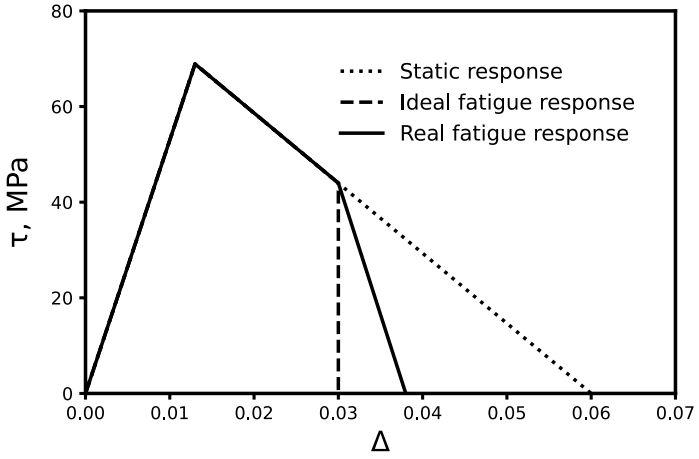

Figure 6. Cohesive traction separation behavior under static and fatigue loading.

TSL for crack tip element is modified by considering the fatigue damage degradation and applying a nonlocal energy release rate approach. With the presence of fatigue damage, the total damage variable is calculated as the sum of static damage variable and fatigue damage variable, as shown in Figure 6.

The fatigue damage variable is derived from the Paris law, as show in the following [19].

$$d_{total}^{k} = d_{s}^{k} + d_{fa}^{k} \tag{1}$$

$$d_{fa}^{k} = d_{fa}^{k-1} + f \cdot \mathrm{d}t \cdot \left(\frac{1-d_{s}^{k}}{L_e}\right) c \left(\frac{G_{his}}{G_{IIc}}\right)^{m} \tag{2}$$

where d represents the damage variable, subscript s and fa denote static and fatigue quantities, respectively. The subscript k denotes current step time. f and $\mathrm{d}t$ denote the persedue frequency and the time increment, respectively. Thus, $f \cdot \mathrm{d}t$ gives the number of elapsed loading cycles of the envelope loading. L_e is the characteristic length of the cohesive element along crack propagation direction. The Paris law parameters c and m have values of 0.12 and 4.38, respectively, for mode II fatigue crack. The historical integrated energy release rate, G_{his}, for the crack tip element is calculated by averaging the values from the 4 integration points as following,

$$G_{his} = \left(\sum_{IP=1}^{4} G_{\max,IP}^{(inst)}\right)/4 \tag{3}$$

where $G_{\max}^{(inst)}$ is the instant integrated energy release rate of the integration point.

Additionally, the non-local energy release rate approach is applied to obtain the maximum field energy release rate. Following the failure of the crack tip element, its neighbor elements are identified as the new crack tip elements and undergo fatigue damage accumulation.

Results and Discussion

Comparison of crack front location between experimental and modelling are seen in Figure 7. The figure gives insights into how accurate and valid the experimental results are when compared to

the modelling results in ABAQUS following the cohesive zone model. Plots for stress ratios R = 0.1 and R = 0.5 depict great accuracy, as also validated in Figure 8 and Figure 9. Plot for stress ratio R = 0.3 depicts a greater fluctuation between the results, as also shown in Figure 8 and Figure 9. This is due to sample slippage that occurred during the test which could have altered the loading condition affecting the stress distribution and crack driving force, leading to possible errors in crack growth rates as compared to modelling [22]. This issue will be addressed in future work. A new 4-point fixture will be used for future tests which grips specimen during the fatigue test, preventing slippage from occurring.

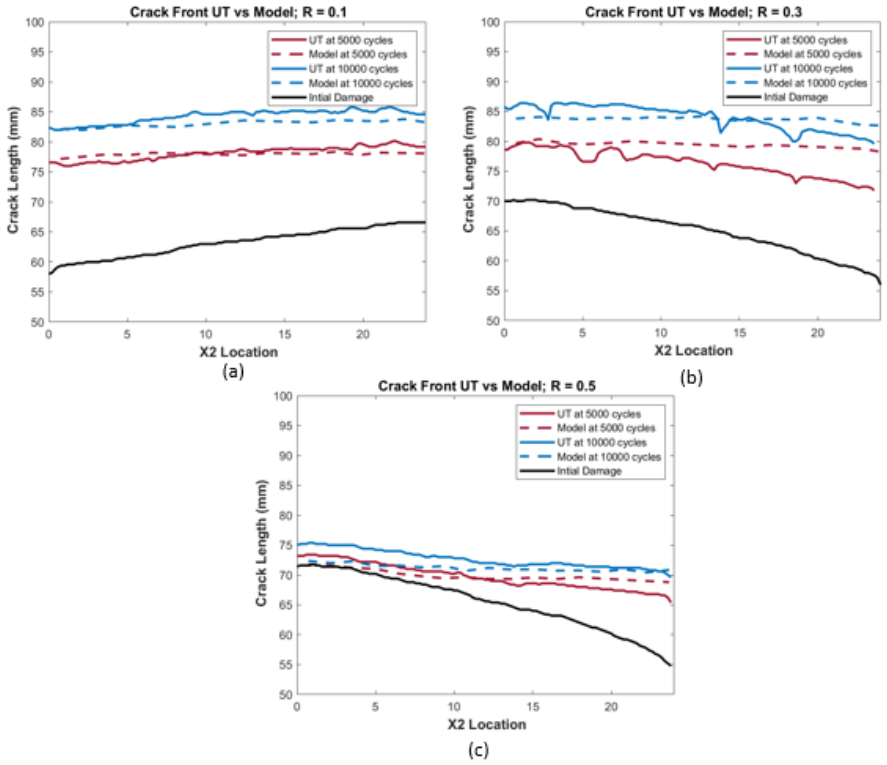

Figure 7. Crack front plotted vs x2 direction for stress ratio (a) 0.1, (b) 0.3 and (c) 0.5.

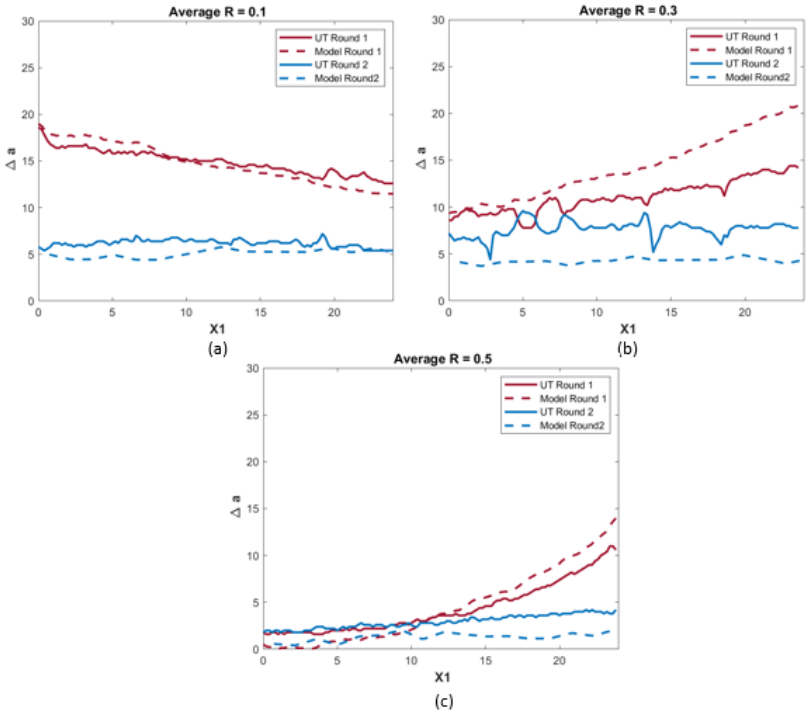

Figure 8. Difference between next iteration – previous iteration of crack front compared vs x2 direction for stress ratio (a) 0.1, (b) 0.3 and (c) 0.5.

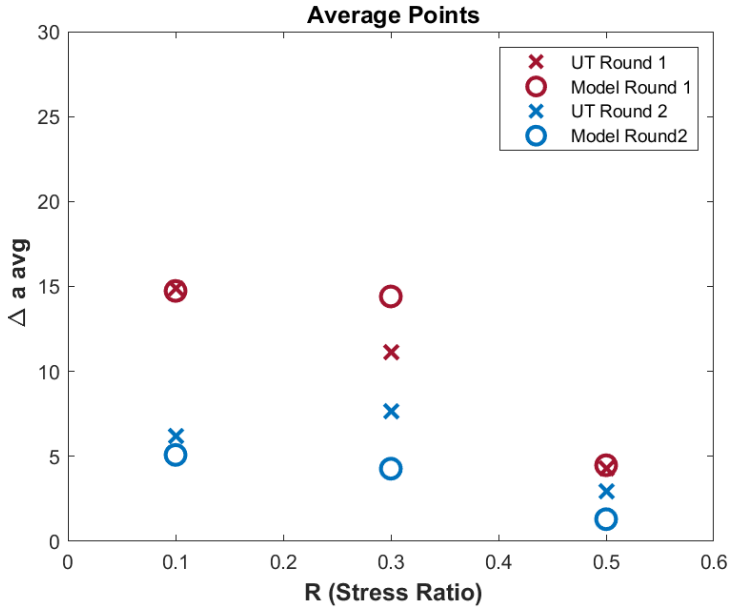

Figure 9. Average points for plots in Figure 5.

Conclusion

This study investigated the experimental testing and modeling of CFRP components under fatigue 4-point bending, focusing on the comparison of the crack front location between the two at predefined numbers of cycles followed by UT scanning and analysis. The results showed good agreement between the experimental and modeling crack fronts which indicates the reliability and

capability of predicting fatigue life via modeling. However, it is important to note that certain limitations such as fixturing, and boundary conditions may have influenced the accuracy during the study as shown in 0.3 stress ratio results. In future work, this will be attended to by using a new fixture which uses clamps to grip the component during testing. This study serves as a foundation for future studies aiming to expand and improve on the reliability of modeling approach.

Acknowledgements

This work was funded by Verifi Technologies.

Bibliography

[1] M. A. Muflikhun, R. Higuchi, T. Yokozeki, and T. Aoki, “Delamination behavior and energy release rate evaluation of CFRP/SPCC hybrid laminates under ENF test: Corrected with residual thermal stresses,” *Composite Structures*, vol. 236, p. 111890, Mar. 2020, doi: 10.1016/j.compstruct.2020.111890.

[2] W. Yuan, Y. Li, and J. Zhao, “Mechanical properties of a novel Tri-directional carbon-flax-aramid fiber reinforced composite,” *Composites Science and Technology*, vol. 213, p. 108923, Sep. 2021, doi: 10.1016/j.compscitech.2021.108923.

[3] S. S. Dash, D. J. Li, X. Q. Zeng, D. Y. Li, and D. L. Chen, “Cyclic deformation behavior and fatigue life prediction of an automotive cast aluminum alloy: A new method of determining intrinsic fatigue toughness,” *Fatigue & Fracture of Engineering Materials & Structures*, vol. 45, no. 3, pp. 725–738, 2022, doi: 10.1111/ffe.13629.

[4] J. Wei, R. Niu, Q. Dong, and S. Zhang, “Fretting-slipping fatigue failure mode in planetary gear system,” *International Journal of Fatigue*, vol. 136, p. 105632, Jul. 2020, doi: 10.1016/j.ijfatigue.2020.105632.

[5] B. Wang, S. Zhong, T.-L. Lee, K. S. Fancey, and J. Mi, “Non-destructive testing and evaluation of composite materials/structures: A state-of-the-art review,” *Advances in Mechanical Engineering*, vol. 12, no. 4, p. 1687814020913761, Apr. 2020, doi: 10.1177/1687814020913761.

[6] D. S. V. de Castro, N. Matvieieva, M. Grosso, C. G. Camerini, H. G. Kotik, and H. Heuer, “Evaluation of Mode II Delamination Area by Non-destructive Techniques: Accuracy and Influence on Fracture Toughness Calculation,” *J Nondestruct Eval*, vol. 40, no. 3, p. 58, Jun. 2021, doi: 10.1007/s10921-021-00789-3.

[7] F. I. Baffour *et al.*, “Ultra-high-resolution imaging of the shoulder and pelvis using photon-counting-detector CT: a feasibility study in patients,” *Eur Radiol*, vol. 32, no. 10, pp. 7079–7086, Oct. 2022, doi: 10.1007/s00330-022-08925-x.

[8] A. R. Venkatakrishnan, S. T. Kim, R. Eisawy, F. Pfister, and N. Navab, “Self-Supervised Out-of-Distribution Detection in Brain CT Scans.” arXiv, Nov. 10, 2020. Accessed: May 30, 2023. [Online]. Available: http://arxiv.org/abs/2011.05428

[9] N. J. Blackman, D. A. Jack, and B. M. Blandford, “Improvement in the Quantification of Foreign Object Defects in Carbon Fiber Laminates Using Immersion Pulse-Echo Ultrasound,” *Materials*, vol. 14, no. 11, Art. no. 11, Jan. 2021, doi: 10.3390/ma14112919.

[10] K. Zhang, S. Li, and Z. Zhou, “Detection of disbonds in multi-layer bonded structures using the laser ultrasonic pulse-echo mode,” *Ultrasonics*, vol. 94, pp. 411–418, Apr. 2019, doi: 10.1016/j.ultras.2018.06.005.

[11] X. Cao, X. Qin, H. Li, S. Shang, S. Li, and H. Liu, “Non-ordinary state-based peridynamic fatigue modelling of composite laminates with arbitrary fibre orientation,” *Theoretical and Applied Fracture Mechanics*, vol. 120, p. 103393, Aug. 2022, doi: 10.1016/j.tafmec.2022.103393.

[12] B. L. V. Bak, A. Turon, E. Lindgaard, and E. Lund, “A simulation method for high-cycle fatigue-driven delamination using a cohesive zone model,” *International Journal for Numerical Methods in Engineering*, vol. 106, no. 3, pp. 163–191, 2016, doi: 10.1002/nme.5117.

[13] A. Turon, J. Costa, P. P. Camanho, and C. G. Dávila, “Simulation of delamination in composites under high-cycle fatigue,” *Composites Part A: Applied Science and Manufacturing*, vol. 38, no. 11, pp. 2270–2282, Nov. 2007, doi: 10.1016/j.compositesa.2006.11.009.

[14] P. Robinson, U. Galvanetto, D. Tumino, G. Bellucci, and D. Violeau, “Numerical simulation of fatigue-driven delamination using interface elements,” *International Journal for Numerical Methods*

in Engineering, vol. 63, no. 13, pp. 1824–1848, 2005, doi: 10.1002/nme.1338.
[15] “Simulation of Mixed-Mode I/II Fatigue Crack Propagation in Adhesive Joints with a Modified Cohesive Zone Model: Journal of Adhesion Science and Technology: Vol 25, No 18.” https://www.tandfonline.com/doi/abs/10.1163/016942411X580180 (accessed Jun. 20, 2023).
[16] G. R. Ibrahim, A. Albarbar, and K. F. Brethee, “Progressive failure mechanism of laminated composites under fatigue loading,” *Journal of Composite Materials*, vol. 55, no. 1, pp. 137–144, Jan. 2021, doi: 10.1177/0021998320944990.
[17] S. Jimenez and R. Duddu, “On the parametric sensitivity of cohesive zone models for high-cycle fatigue delamination of composites,” *International Journal of Solids and Structures*, vol. 82, pp. 111–124, Mar. 2016, doi: 10.1016/j.ijsolstr.2015.10.015.
[18] B. L. V. Bak, A. Turon, E. Lindgaard, and E. Lund, “A benchmark study of simulation methods for high-cycle fatigue-driven delamination based on cohesive zone models,” *Composite Structures*, vol. 164, pp. 198–206, Mar. 2017, doi: 10.1016/j.compstruct.2016.11.081.
[19] L. F. Kawashita and S. R. Hallett, “A crack tip tracking algorithm for cohesive interface element analysis of fatigue delamination propagation in composite materials,” *International Journal of Solids and Structures*, vol. 49, no. 21, pp. 2898–2913, Oct. 2012, doi: 10.1016/j.ijsolstr.2012.03.034.
[20] “Standard Test Method for Determination of the Mode II Interlaminar Fracture Toughness of Unidirectional Fiber-Reinforced Polymer Matrix Composites.” https://www.astm.org/d7905_d7905m-19e01.html (accessed May 30, 2023).
[21] P. W. Harper and S. R. Hallett, “A fatigue degradation law for cohesive interface elements – Development and application to composite materials,” *International Journal of Fatigue*, vol. 32, no. 11, pp. 1774–1787, Nov. 2010, doi: 10.1016/j.ijfatigue.2010.04.006.
[22] R. Mohammadi, M. A. Najafabadi, H. Saghafi, M. Saeedifar, and D. Zarouchas, “The effect of mode II fatigue crack growth rate on the fractographic features of CFRP composite laminates: An acoustic emission and scanning electron microscopy analysis,” *Engineering Fracture Mechanics*, vol. 241, p. 107408, Jan. 2021, doi: 10.1016/j.engfracmech.2020.107408.